

A Bayesian multivariate extreme value mixture model

Chenglei Hu^{1*}, Ben Swallow² and Daniela Castro-Camilo¹

January 30, 2024

Abstract

Impact assessment of natural hazards requires the consideration of both extreme and non-extreme events. Extensive research has been conducted on the joint modeling of bulk and tail in univariate settings; however, the corresponding body of research in the context of multivariate analysis is comparatively scant. This study extends the univariate joint modeling of bulk and tail to the multivariate framework. Specifically, it pertains to cases where multivariate observations exceed a high threshold in at least one component. We propose a multivariate mixture model that assumes a parametric model to capture the bulk of the distribution, which is in the max-domain of attraction (MDA) of a multivariate extreme value distribution (mGEVD). The tail is described by the multivariate generalized Pareto distribution, which is asymptotically justified to model multivariate threshold exceedances. We show that if all components exceed the threshold, our mixture model is in the MDA of an mGEVD. Bayesian inference based on multivariate random-walk Metropolis-Hastings and the automated factor slice sampler allows us to incorporate uncertainty from the threshold selection easily. Due to computational limitations, simulations and data applications are provided for dimension $d = 2$, but a discussion is provided with views toward scalability based on pairwise likelihood.

Keywords: extreme mixture models; joint modeling of bulk and tail; multivariate generalized Pareto distribution

¹School of Mathematics and Statistics, University of Glasgow, UK.

²School of Mathematics and Statistics, University of St Andrews, UK.

*Corresponding author. Email address: c.hu.2@research.gla.ac.uk

1 Introduction

Extreme value theory (EVT) provides probabilistic results and statistical tools to model and predict extreme outcomes, helping us prepare for and mitigate rare but impactful events, such as financial market crashes, natural disasters, or structural failures. The risk associated with extremes is usually compound, and therefore, the focus is on problems that involve the concurrence of multiple extreme events, such as heavy rainfall and extreme wind speed, different pollutants above regulatory standards, or multiple stock markets reporting losses at the same time. One common way to define extreme events for a single variable is through the peaks over threshold (PoT) method suggested by [Pickands \(1975\)](#) and later formalized by [Davison and Smith \(1990\)](#). It relies on the asymptotic property that for a high enough threshold, the conditional distribution of threshold exceedances follows a generalized Pareto distribution (GPD) if the random variable is in the max-domain of attraction (MDA) of a generalized extreme value distribution (GEVD, also called max-stable distribution). The MDA condition implies that the properly renormalized block maxima vector converges to a GEVD as the number of blocks increases. For multiple variables, the PoT method extends naturally by choosing a high threshold for each variable, but the definition of exceedances of a multivariate threshold is not unique. One widely used definition is that provided by [Rootzén and Tajvidi \(2006\)](#), which relies on at least one of the components exceeding its corresponding threshold. Nonetheless, independent of the definition used, asymptotic theory for exceedances of a multivariate threshold does not offer a finite parametrization of the limiting distribution.

Over the last few years, different authors have proposed methods that combine statistics of extremes with classical statistical models for the bulk or body of the distribution. In the univariate setting, [Frigessi et al. \(2002\)](#) proposed a dynamically weighted mixture model, combining the GPD with a lighter-tailed distribution, ensuring that the GPD predominantly influences the tail. [Behrens et al. \(2004\)](#) made the threshold a parameter and characterized the data above the threshold with the GPD and the remainder with a suitable parametric distribution. Building upon Behrens's foundational work, [Tancredi et al. \(2006\)](#) and [do Nascimento et al. \(2012\)](#) employed semi-parametric approaches to approximate the central data, whereas [MacDonald et al. \(2011\)](#) applied non-parametric approaches. [Huang et al. \(2019\)](#) explored the full range of the data by fitting a cubic spline on the binned histogram of log-transformed observations,

resulting in a polynomial tail estimation. [Naveau et al. \(2016\)](#) and [Stein \(2021\)](#) constructed a single distribution that mimics the GPD in both its lower and upper tails through compositions of distributions, while [Krock et al. \(2022\)](#) expanded Stein’s model to the non-stationary scenarios. More recently, [Opitz et al. \(2018\)](#) and [Castro-Camilo et al. \(2019\)](#) used (discontinuous) spliced models to describe both the bulk and tail of different environmental variables over space and time to improve the prediction and forecasting of extreme events.

In the bivariate setting, [Leonelli and Gaman \(2020\)](#) utilized an extreme value mixture model in conjunction with a mixture of copulae to facilitate estimations of both the margins and the dependence structures. [Aulbach et al. \(2012a\)](#) devised a method wherein the upper tail region of a copula was truncated and subsequently merged with a multivariate GPD copula. The exact representation of the upper tail of this piecing-together approach was given by [Aulbach et al. \(2012b\)](#). This approach was further elaborated upon by [André et al. \(2024\)](#), who blended copulae specifically designed for tail and bulk regions, ensuring a seamless transition between the two.

This paper introduces a comprehensive framework for multivariate modeling of bulk and tail via mixtures that build upon the univariate extreme mixture model proposed by [Behrens et al. \(2004\)](#). Our mixture model combines a parametric distribution for the bulk in the MDA of a multivariate generalized extreme value distribution (mGEVD) with a multivariate generalized Pareto Distribution (mGPD) for an accurate description of the multivariate tail. Due to the simplicity of construction, simulation from our model is straightforward. Contrary to the approaches in [Aulbach et al. \(2012b,a\)](#) and [André et al. \(2024\)](#), we here adopt a Bayesian approach for inference where the selection and uncertainty of the multivariate threshold are automatically integrated into the estimation process. Specifically, we use a multivariate random-walk Metropolis-Hastings (MH) with dynamically calibrated MH scaling parameter (as discussed by [Roberts and Rosenthal 2001](#)) and an automated factor slice sampler ([Tibbits et al., 2014](#)) to address suboptimal mixing for certain parameters. A distinct advantage of our framework is the robust justification of the tail behavior based on the asymptotic properties of the mGPD. Moreover, we provide a formal characterization of the extreme behavior of our mixture model, showing that our model is in the MDA of an mGEVD if all components exceed the threshold. We test the performance of our model under well-specified scenarios with different degrees of marginal tail heaviness and misspecified scenarios where data are assumed to come from an

asymptotically independent model. We compare our model with that of [André et al. \(2024\)](#) using a best-performing copulae configuration and show that our model accurately captures bulk and tail dependencies. We illustrate the applicability of our model using temperature records in the UK that show the need to describe the joint tail behavior accurately.

The rest of the paper is structured as follows. Section 2 introduces our model for $d \geq 2$ variables, including a comprehensive background of the mGPD construction and our chosen mGPD representation. Section 3 discusses the priors used for the model parameters and outlines the methodology for posterior inference. A simulation study to validate our model is carried out in Section 4 while Section 5 illustrates our model on a UK temperature dataset, demonstrating superior estimation capabilities in comparison to conventional techniques. Due to the nature of our model, simulation and data application are provided for $d = 2$ dimensions. Therefore, in Section 6, we provide a discussion on the use of our model for higher dimensions using Bayesian inference based on pairwise likelihood.

2 Multivariate extreme mixture model

2.1 Multivariate generalized Pareto distribution

Let $\mathbf{Y}_1, \dots, \mathbf{Y}_n$ be n independent and identical copies of the d -dimensional random vector \mathbf{Y} , which is in the MDA of an mGEVD G . This means that there exists sequences of normalising vectors $\mathbf{a}_n \in (0, \infty)^d$ and $\mathbf{b}_n \in \mathbb{R}^d$ such that

$$\mathbb{P} \left(\mathbf{a}_n \left\{ \max_{1 \leq i \leq n} \mathbf{Y}_i \right\} + \mathbf{b}_n \leq \mathbf{y} \right) = \mathbb{P}^n (\mathbf{a}_n \mathbf{Y} + \mathbf{b}_n \leq \mathbf{y}) \rightarrow G(\mathbf{y}), \quad n \rightarrow \infty. \quad (1)$$

Here, operations on vectors are componentwise. For example, $\mathbf{a}_n \mathbf{Y} + \mathbf{b}_n = (a_{n,1}Y_1 + b_{n,1}, \dots, a_{n,d}Y_d + b_{n,d})$ and $\max_{1 \leq i \leq n} \{\mathbf{Y}_i\} = (\max_{1 \leq i \leq n} \{Y_{i,1}\}, \dots, \max_{1 \leq i \leq n} \{Y_{i,d}\})$. $G(\mathbf{y})$ is an mGEVD with non-degenerating margins $G_j(x)$, $j = 1, \dots, d$ belonging to the univariate generalized extreme value family of distributions. Without loss of generality, we can assume that marginals are unit Fréchet with cumulative distribution function $\exp(y^{-1})$, for $y > 0$. In that case, we can write the joint distribution function G as

$$G(\mathbf{y}) = \exp \{-V(\mathbf{y})\} = \exp \left\{ - \int_{S_d} \max \left(\frac{w_1}{y_1}, \dots, \frac{w_d}{y_d} \right) dQ(\mathbf{w}) \right\}, \quad \mathbf{y} > \mathbf{0}. \quad (2)$$

Q is called the spectral measure, an arbitrary positive finite measure over the unit simplex $\mathcal{S}_d = \{\mathbf{w} \in [0, 1]^d : \sum_{j=1}^d w_j = 1\}$ that satisfies the constraint

$$\int_{\mathcal{S}_d} w_j dQ(\mathbf{w}) = 1, \quad j = 1, \dots, d.$$

Let $\mathbf{Y} \not\leq \mathbf{b}_n$ denote the event of at least one of the \mathbf{Y} components exceeding the corresponding \mathbf{b}_n component. If the convergence in (1) holds, the conditional random vector defined as

$$\max \left\{ \frac{\mathbf{Y} - \mathbf{b}_n}{\mathbf{a}_n}, \boldsymbol{\eta}^l \right\} \Big| \mathbf{Y} \not\leq \mathbf{b}_n \quad (3)$$

converges in distribution to a d -dimensional random vector \mathbf{X} with multivariate generalized Pareto distribution (mGPD) H . In (3), $\boldsymbol{\eta}^l$ is the vector of lower end points of H whose components η_j^l depend on the conditional marginal parameters in (5). Rootzén and Tajvidi (2006) showed that H is associated with G , and it can be expressed as

$$H(\mathbf{x}) = \frac{1}{\log G(\mathbf{0})} \log \frac{G(\mathbf{x} \wedge \mathbf{0})}{G(\mathbf{x})}, \quad \mathbf{x} > \boldsymbol{\eta}^l, \quad (4)$$

where \wedge denotes the componentwise minimum and $0 < G(\mathbf{0}) < 1$ is assumed. Contrary to the mGEVD, marginal distributions of $H(\mathbf{x})$ do not conform to univariate GPDs since $\mathbf{Y} \not\leq \mathbf{b}_n$ does not necessarily imply that $Y_j > b_j$ for every j . But if $X_j > 0$, the corresponding conditional marginal distributions H_j are indeed GPD, i.e.,

$$\mathbb{P}(X_j > x_j | X_j > 0) = 1 - \frac{H_j(x) - H_j(0)}{1 - H_j(0)} = \left(1 + \gamma_j \frac{x_j}{\sigma_j} \right)^{-1/\gamma_j}, \quad x_j > 0. \quad (5)$$

The lower endpoint η_j^l and upper endpoint η_j^u of H_j are $\eta_j^l = -\sigma_j/\gamma_j$ and $\eta_j^u = +\infty$ for $\gamma_j > 0$, $\eta_j^l = -\infty$ and $\eta_j^u = -\sigma_j/\gamma_j$ for $\gamma_j < 0$, and $\eta_j^l = -\infty$ and $\eta_j^u = +\infty$ for $\gamma_j = 0$. As we can see from (2) and (4), both the mGEVD and the mGPD depend on the spectral measure Q and therefore have no unique representation. Based on the work by Rootzén et al. (2018), Kiriliouk et al. (2019) introduce three constructions to develop parametric models for the density of the mGPD. Here, we use the so-called U representation with density

$$h_{\mathbf{U}}(\mathbf{x}) = \mathbb{1}\{\max(\mathbf{x}) > 0\} \frac{\prod_{i=1}^d (\gamma_i x_i + \sigma_i)^{-1}}{\mathbb{E}[\exp(\max(\mathbf{U}))]} \int_0^\infty f_{\mathbf{U}} \left(\frac{1}{\boldsymbol{\gamma}} \log \left(\frac{\boldsymbol{\gamma}}{\boldsymbol{\sigma}} \mathbf{x} + \mathbf{1} \right) + \log t \right) dt, \quad (6)$$

where $f_{\mathbf{U}}$ is the density of a random vector \mathbf{U} satisfying $\mathbb{E}[\exp(U_j)] < +\infty, j = 1, \dots, d$ and $[\log(\gamma_j x_j / \sigma_j + 1)] / \gamma_j$ takes its limiting form x_j / σ_j when $\gamma_j = 0$. A standardized form of (6) with $\boldsymbol{\gamma} = \mathbf{0}$ and $\boldsymbol{\sigma} = \mathbf{1}$ can be obtained by applying the transformation

$$\mathbf{Z} := \frac{1}{\boldsymbol{\gamma}} \log \left(\frac{\boldsymbol{\gamma}}{\boldsymbol{\sigma}} \mathbf{X} + \mathbf{1} \right), \quad (7)$$

where the random vector \mathbf{X} has the density in (6). As a result, the standardized density can be expressed as

$$h_{\mathbf{U}}(\mathbf{z}) = \mathbb{1}\{\max(\mathbf{z}) > 0\} \frac{1}{\mathbb{E}[\exp(\max(\mathbf{U}))]} \int_0^\infty f_{\mathbf{U}}(\mathbf{z} + \log t) dt. \quad (8)$$

In practice, the mGPD is usually first defined on the standardized scale given in (8) and then transformed back to the observation scale using (7). Note that the U density in (6) or (8) still lacks finite parametrization since it depends on the density function $f_{\mathbf{U}}$, which determines the extremal dependence of the mGPD. In the rest of this paper, we assume that \mathbf{U} has independent reverse exponential components, that is $f_{\mathbf{U}}(\mathbf{x}) = \prod_{i=1}^d a_i^{-1} \exp(a_i^{-1} x_i)$, for $x_i \in (-\infty, 0)$, $a_i > 0$; hence, (8) can be explicitly expressed as

$$h_{\mathbf{U}}(\mathbf{z}) = \frac{\exp[-\max(\mathbf{z})(1 + \sum_{i=1}^d a_i^{-1})] \prod_{i=1}^d a_i^{-1} \exp(a_i^{-1} z_i)}{\mathbb{E}[\exp(\max(\mathbf{U}))] (1 + \sum_{i=1}^d a_i^{-1})}, \quad (9)$$

where $\mathbb{E}[\exp(\max(\mathbf{U}))] = \int_0^\infty 1 - \mathbb{P}(\exp(\max(\mathbf{U})) \leq t) dt = (\sum_{i=1}^d a_i^{-1}) / (1 + \sum_{i=1}^d a_i^{-1})$.

2.2 Multivariate bulk distribution

The mGPD in Section 2.1 is defined within the complement of the negative orthant. Incorporating the threshold vector \mathbf{u} , this specific region undergoes a transition to the designated region A , where at least one component exceeds the threshold, formally represented as $A = \{\mathbf{x} \in \mathbb{R}^d : \mathbf{x} - \mathbf{u} \not\leq \mathbf{0}\}$. For the region $\mathbb{R}^d \setminus A$, we assume observations come from a multivariate distribution F_{bulk} on \mathbb{R}^d with density function f_{bulk} . For the mGPD to be a suitable description of the tail of F_{bulk} , we further assume the F_{bulk} is within the MDA of the mGEVD G . The sufficient conditions for a multivariate distribution to be in the MDA of an mGEVD have been articulated by Yun (1997). This includes several examples, such as the multivariate exponential distribution, multivariate t-distribution, multivariate gamma distribution, and multivariate normal distribution. The choice of the multivariate bulk distribution F_{bulk} is flexible and depends on the properties of the system under study; in the rest of the paper, we assume that F_{bulk} is the multivariate normal distribution, but other multivariate distributions could easily be assumed. Hence, the density of the bulk distribution is

$$f_{\text{bulk}}(\mathbf{x} | \boldsymbol{\mu}, \boldsymbol{\Sigma}) = (2\pi)^{-d/2} (\det \boldsymbol{\Sigma})^{-\frac{1}{2}} \exp \left\{ -\frac{1}{2} (\mathbf{x} - \boldsymbol{\mu})' \boldsymbol{\Sigma}^{-1} (\mathbf{x} - \boldsymbol{\mu}) \right\}, \quad \mathbf{x} \leq \mathbf{u}, \quad (10)$$

where $\boldsymbol{\mu}$ is the mean vector and $\boldsymbol{\Sigma}$ is the covariance matrix.

2.3 Multivariate extreme mixture distribution

Since the tail and bulk define a partition of the mixture model's support, combining (10) and (9), the density function of our multivariate extreme mixture model can be written as

$$f(\mathbf{x}|\boldsymbol{\mu}, \boldsymbol{\Sigma}, \mathbf{a}, \boldsymbol{\sigma}, \boldsymbol{\gamma}, \mathbf{u}) = \begin{cases} f_{\text{bulk}}(\mathbf{x}|\boldsymbol{\mu}, \boldsymbol{\Sigma}), & \text{if } \mathbf{x} \leq \mathbf{u} \\ [1 - F_{\text{bulk}}(\mathbf{u}|\boldsymbol{\mu}, \boldsymbol{\Sigma})]h_{\mathcal{U}}(\mathbf{x} - \mathbf{u}|\mathbf{a}, \boldsymbol{\sigma}, \boldsymbol{\gamma}), & \text{otherwise.} \end{cases} \quad (11)$$

The density in (11) indicates that data are characterized by the multivariate normal distribution when all components are less than the threshold \mathbf{u} and described by the U-representation of the mGPD with a reverse exponential generator when at least one component exceeds the threshold. We can write (11) in terms of the usual mixture distribution representation using the truncated bulk density $f_{\text{bulk}}^*(\mathbf{x}|\boldsymbol{\mu}, \boldsymbol{\Sigma}) = \mathbb{1}\{\mathbf{x} \leq \mathbf{u}\}f_{\text{bulk}}(\mathbf{x}|\boldsymbol{\mu}, \boldsymbol{\Sigma})/F_{\text{bulk}}(\mathbf{u}|\boldsymbol{\mu}, \boldsymbol{\Sigma})$. Our extreme mixture model can then be expressed as

$$f(\mathbf{x}|\boldsymbol{\mu}, \boldsymbol{\Sigma}, \mathbf{a}, \boldsymbol{\sigma}, \boldsymbol{\gamma}, \mathbf{u}) = \pi f_{\text{bulk}}^*(\mathbf{x}|\boldsymbol{\mu}, \boldsymbol{\Sigma}) + (1 - \pi)h_{\mathcal{U}}(\mathbf{x} - \mathbf{u}|\mathbf{a}, \boldsymbol{\sigma}, \boldsymbol{\gamma}),$$

where the mixture probability is $\pi = F_{\text{bulk}}(\mathbf{u}|\boldsymbol{\mu}, \boldsymbol{\Sigma})$. We argue that this representation makes our model construction very intuitive, and it is preferred for the implementation of our sampling algorithm described in Section 3.

To visualize our model, Figure 1 depicts a two-dimensional representation of the density in (11). The dashed segments at $X_1 = u_1$ and $X_2 = u_2$ demarcate the boundary between the bulk and the tail, as well as the discontinuities within the density function. This is evidenced by the abrupt alteration in the density contour lines upon traversing this boundary. Furthermore, we can also visualize the marginal densities; consider, for instance, the density of X_1 in the left-hand plot. When $X_1 > u_1 = 5.7$, the marginal density is entirely constituted by the bivariate GPD, indicated by the triangular lines. Conversely, when $X_1 < 5.7$, the marginal density becomes a mixture of both the bivariate GPD (triangular lines) and the bivariate normal distribution (elliptical lines). This means that although the bulk follows a multivariate normal distribution, the marginal bulk distribution $f_i(x_i|x_i < u_i)$ is generally not normally distributed.

As we can see from (11), the tail behavior of our model is completely determined by the mGPD; therefore, our multivariate extreme mixture model has solid theoretical foundations to

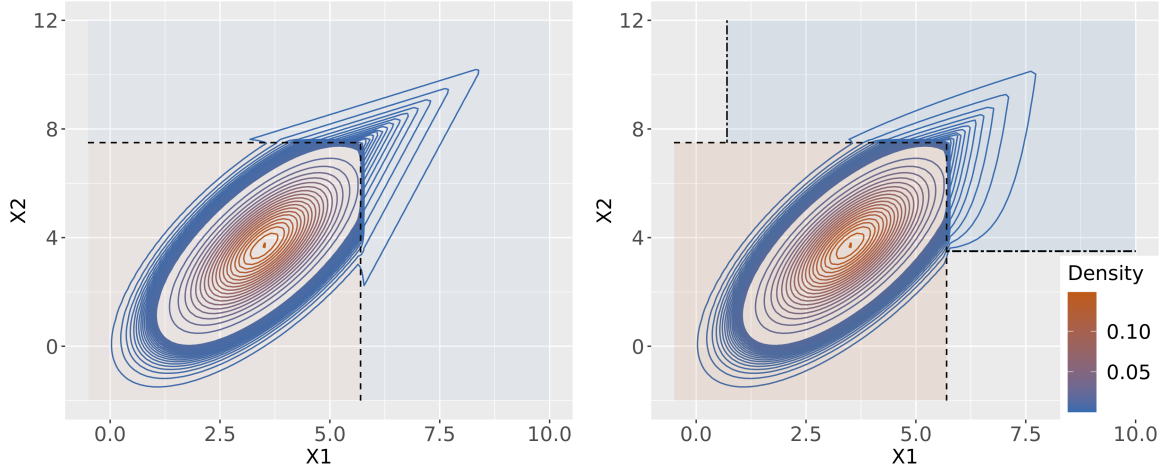


Figure 1: Two-dimensional density contour plots derived from (11). Dashed lines indicate threshold values, whereas the double-dashed lines in the right plot highlight the lower endpoints of the bivariate GPD. Shaded areas represent the support of each mixture component. For the left plot, the bivariate GPD parameters are specified as $\sigma = \mathbf{1}$, $\gamma = \mathbf{0}$, and $\mathbf{a} = (1, 2)$. Conversely, the right plot employs parameters $\sigma = (1, 1.2)$, $\gamma = (0.2, 0.3)$, and $\mathbf{a} = (1, 2)$. Notably, both plots share common parameters for the bulk and threshold, represented by $\boldsymbol{\mu} = (3.5, 3.7)$, $\boldsymbol{\Sigma} = \begin{pmatrix} 1 & 1.05 \\ 1.05 & 2.25 \end{pmatrix}$, and $\mathbf{u} = (5.7, 7.5)$.

describe multivariate extremes. Properties of the mGPD, such as GPD conditional margins, are transferred to our model. Furthermore, extremal dependence can be directly characterized by h_U , and if all component exceeds the threshold, our model is in the MDA of an mGEVD. This last result is stated in the following proposition, and its proof is deferred to the appendix.

Proposition 1. *Let F be a distribution with a density function as defined in (11). Then, its MDA falls in the following two cases:*

1. *If all components exceed the threshold, F is in the MDA of some mGEVD.*
2. *Conversely, if no components or only part of the components exceed the threshold, F is not in the MDA of any mGEVD.*

3 Bayesian Inference

Although maximum likelihood-based inference can in principle be adopted using, e.g., a version of the EM algorithm for mixture models, the Bayesian paradigm offers a natural way to address all sources of uncertainty from our model, including that of the threshold selection. Here, we

detail prior selection for all the parameters of our model, namely $\boldsymbol{\mu}$, $\boldsymbol{\Sigma}$ for the bulk, the threshold \mathbf{u} and \mathbf{a} , $\boldsymbol{\gamma}$ and $\boldsymbol{\sigma}$ for the tail.

3.1 Priors for the parameters in the bulk

A common approach in assigning priors for the multivariate normal distribution parameters involves using a multivariate normal prior for the mean vector and an inverse-Wishart distribution for the covariance matrix. While this methodology offers conjugacy, it often falls short in providing the requisite flexibility for the covariance matrix, as highlighted by [Sun and Berger \(2007\)](#). To address this limitation, [Barnard et al. \(2000\)](#) proposed a prior specification on the decomposition of the covariance matrix expressed as $\boldsymbol{\Sigma} = \text{diag}(\mathbf{S})\mathbf{C}\text{diag}(\mathbf{S})$, where \mathbf{C} denotes the d -dimensional correlation matrix, and \mathbf{S} represents the $d \times 1$ standard deviation vector. This approach advocates for specifying priors for these individual components. In our simulation and case study in Sections 4 and 5, we assign independent uniform priors $U(0, b_i)$ for each element s_i in \mathbf{S} , with an adequately large upper bound b_i . We found that to provide an uninformative prior, it is enough to choose b_i to be 50 times as large as the data scale. Concurrently, the prior for the correlation matrix is designated as a Lewandowski-Kurowicka-Joe (LKJ) distribution, as per [Lewandowski et al. \(2009\)](#), with the specific formulation $\pi(\mathbf{C}) \propto (\det \mathbf{C})^{\delta-1}$. The δ parameter, intrinsic to the LKJ distribution, regulates correlation strength. A δ value of 1 yields a density uniform over all d -dimensional correlation matrices due to the density's proportionality to a constant. For $\delta > 1$, the matrix with stronger diagonal elements (implying stronger correlation) is favored. Conversely, $\delta < 1$ indicates a preference for a weak diagonal matrix. In consideration of the computational efficiency, we work with the upper triangular Cholesky factor \mathbf{U} of the correlation matrix, where $\mathbf{C} = \mathbf{U}^T\mathbf{U}$, rather than \mathbf{C} itself. The prior $\pi(\mathbf{U}; \delta)$ is derived from $\pi(\mathbf{C})$ and is thus parameterized by δ . For the mean vector $\boldsymbol{\mu}$, we use the standard approach and assume that each element μ_i follows a normal prior $N(m_i, t_i^2)$, independent of each other. In summary, the prior for the bulk is as follows:

$$\pi(\boldsymbol{\mu}, \boldsymbol{\Sigma}) = \pi(\boldsymbol{\mu}, \mathbf{S}, \mathbf{U}) \propto |\mathbf{U}^T\mathbf{U}|^\delta \prod_{i=1}^d \frac{1}{\sqrt{2\pi}} \exp\left\{-\frac{1}{2}\left(\frac{\mu_i - m_i}{t_i}\right)^2\right\} \cdot \mathbb{1}(0 < s_i < b_i). \quad (12)$$

3.2 Prior for the threshold

The threshold plays a critical role in the threshold exceedance framework. A high threshold leaves few points for exceedance estimation, leading to a higher variance of parameter estimates. In contrast, a low threshold can violate the asymptotic assumption of the mGPD, which leads to biased estimates. Following [Behrens et al. \(2004\)](#), we assume that the marginal threshold u_i independently follows a truncated normal distribution, and the prior for the threshold is

$$\pi(\mathbf{u}|\boldsymbol{\nu}_u, \mathbf{s}_u, \mathbf{p}_u, \mathbf{q}_u) \propto \prod_{i=1}^d \varphi\left(\frac{u_i - \nu_{u,i}}{s_{u,i}}\right) \cdot \mathbb{1}(p_{u,i} \leq u_i \leq q_{u,i}), \quad (13)$$

where φ is the density of a standard normal random variable, $\boldsymbol{\nu}_u = (\nu_{u,1}, \dots, \nu_{u,d})$ and $\mathbf{s}_u = (s_{u,1}, \dots, s_{u,d})$ are the mean and standard deviation of the truncated normal, respectively, and $\mathbf{p}_u = (p_{u,1}, \dots, p_{u,d})$ and $\mathbf{q}_u = (q_{u,1}, \dots, q_{u,d})$ are the lower and upper bounds of its support. Our objective is to maintain the threshold within a high quantile yet with sufficient adaptability to ascertain the optimal value derived from the data and account for reasonable uncertainty. We establish $p_{u,i}$ and $q_{u,i}$ at high data percentiles, selecting the 80th and 99th percentiles of the margin, respectively. Meanwhile, $\nu_{u,i}$ is positioned at another elevated percentile, specifically the 90th percentile in both our simulations and application in [Sections 4 and 5](#). The parameter $s_{u,i}$ is assigned a sufficiently large value relative to the data, thereby exhibiting a non-informative prior over $[p_{u,i}, q_{u,i}]$. Alternatively, a continuous uniform could be assumed. The principal aim is to ensure a balance between allowing for realistic uncertainty, whilst maintaining sufficient data above and below the threshold to reliably estimate the relevant parameters.

3.3 Priors for the parameters in the tail

The marginal parameters in the mGPD are represented as $\boldsymbol{\gamma} = (\gamma_1, \dots, \gamma_d)$ and $\boldsymbol{\sigma} = (\sigma_1, \dots, \sigma_d)$. Their interpretation aligns closely with the univariate GPD, given that the marginal conditional distribution $H_i(x_i|x_i > 0)$ of the mGPD is a univariate GPD. [Coles and Powell \(1996\)](#) suggested utilizing expert knowledge of return level to establish a gamma prior for the quantile difference. This prior was subsequently used to derive the priors for $\boldsymbol{\gamma}$ and $\boldsymbol{\sigma}$. Conversely, [Castellanos and Cabras \(2007\)](#) introduced the Jeffreys prior for the univariate GPD. In our framework, we assume that the γ_j independently follows a uniform distribution $U(l_\gamma, u_\gamma)$ and σ_j independently follows a uniform distribution $U(l_\sigma = 0, u_\sigma)$, where $l_{(\cdot)}$ and $u_{(\cdot)}$

represents the lower bound and upper bound for each parameter. Furthermore, the parameter $\mathbf{a} = (a_1, \dots, a_d)$ defined in (9) that governs the tail dependence structure is assumed uniformly distributed between 0 and u_a . In summary, the joint prior distribution for the tail parameters is as follows

$$\pi(\mathbf{a}, \gamma, \boldsymbol{\sigma}) \propto \prod_{i=1}^d \mathbb{1}(0 < a_i < u_a) \cdot \mathbb{1}(l_\gamma < \gamma_i < u_\gamma) \cdot \mathbb{1}(0 < \sigma_i < u_\sigma). \quad (14)$$

3.4 Posterior Inference

Let $\boldsymbol{\theta}_1 = (\boldsymbol{\mu}, \mathbf{S}, \mathbf{U})$, $\boldsymbol{\theta}_2 = \mathbf{u}$, and $\boldsymbol{\theta}_3 = (\mathbf{a}, \gamma, \boldsymbol{\sigma})$. Let $\mathbf{X} = (\mathbf{x}_1, \dots, \mathbf{x}_n)^t$ be an $n \times d$ sample matrix. Define the mutually exclusive sets B and T to be the indices of \mathbf{X} associated with bulk and tail data, taking values in $\{1, \dots, n\}$. The log posterior density of our multivariate extreme mixture model in (11) is given by:

$$\begin{aligned} \log \pi(\boldsymbol{\theta}_1, \boldsymbol{\theta}_2, \boldsymbol{\theta}_3 | \mathbf{X}) &\propto \sum_{i=1}^n \log \{ f_{\text{bulk}}(\mathbf{x}_i | \boldsymbol{\theta}_1) \cdot \mathbb{1}(\mathbf{x}_i \leq \boldsymbol{\theta}_2) \\ &\quad + [1 - F_{\text{bulk}}(\boldsymbol{\theta}_2 | \boldsymbol{\theta}_1)] f_{\text{tail}}(\mathbf{x}_i - \boldsymbol{\theta}_2 | \boldsymbol{\theta}_3) \cdot \mathbb{1}(\mathbf{x}_i \not\leq \boldsymbol{\theta}_2) \} \\ &\quad + \log \pi(\boldsymbol{\theta}_1) + \log \pi(\boldsymbol{\theta}_2) + \log \pi(\boldsymbol{\theta}_3) \\ &\propto \sum_{i \in B} \log f_{\text{bulk}}(\mathbf{x}_i | \boldsymbol{\theta}_1) + \sum_{i \in T} \log f_{\text{tail}}(\mathbf{x}_i - \boldsymbol{\theta}_2 | \boldsymbol{\theta}_3) \} + |T| \log[1 - F_{\text{bulk}}(\boldsymbol{\theta}_2 | \boldsymbol{\theta}_1)] \\ &\quad + \log \pi(\boldsymbol{\theta}_1) + \log \pi(\boldsymbol{\theta}_2) + \log \pi(\boldsymbol{\theta}_3), \end{aligned} \quad (15)$$

where $|T| = |T(\boldsymbol{\theta}_2)|$ is the number of elements in the set T and implicitly depends on the threshold $\boldsymbol{\theta}_2$. Inference is conducted via Markov Chain Monte Carlo (MCMC) methods to draw samples from the posterior distribution as described in (15). Initially, we utilize the multivariate random-walk Metropolis-Hastings (MH) algorithm for sampling purposes. Each parameter is associated with an independent normal proposal. The scaling parameter within the proposal density is dynamically calibrated to achieve the theoretical optimal acceptance rate, as discussed by [Roberts and Rosenthal \(2001\)](#). However, we occasionally encounter suboptimal mixing for the parameters $\boldsymbol{\theta}_2$ and certain elements of $\boldsymbol{\theta}_3$, attributable to the inherent dependencies among the parameters. For instance, an increased threshold u_i typically corresponds to a reduced marginal scale σ_i when the marginal data scale is fixed. To address these dependencies and enhance sampling efficiency, we apply the automated factor slice sampler (AFSS)

introduced by [Tibbits et al. \(2014\)](#). The AFSS method mitigates parameter correlation by implementing univariate slice sampling along the covariance matrix’s eigenvectors derived from the target distribution’s quadratic approximation. This technique has demonstrated a substantial increase in computational efficiency, often exceeding 10-fold improvements, as gauged by the ratio of effective sample size to running time. For practical implementation and expedited computation, both the random-walk and AFSS samplers have been integrated and executed within the R environment using the Nimble package ([de Valpine et al., 2017](#)), which facilitates straightforward C++ compilation.

4 Simulations

Simulation studies are conducted to assess the performance of our model across diverse scenarios. For these simulations, we constrain the dimensionality to two. Our simulation scenarios explore the marginal tails’ behavior under varying degrees of tail heaviness. Specifically, scenarios 1.1 through 1.3 encompass configurations with two heavy-tailed margins ($\gamma_1 = 0.3, \gamma_2 = 0.1$), a combination of one heavy-tailed and one light-tailed margin ($\gamma_1 = 0.2, \gamma_2 = -0.2$), and two light-tailed margins ($\gamma_1 = -0.1, \gamma_2 = -0.3$), respectively. All other parameters are consistent across these scenarios, as detailed in the TV (True Value) columns of [Tables 1 and 2](#). Each scenario involves a simulation of 2,000 data points, with approximately 5% constituting the tail data.

Priors are established to be uninformative, characterized by $\delta = 1.3, m_1 = m_2 = 0, b_1 = b_2 = 50$ in [\(12\)](#), while $\nu_{u,i}, p_{u,i}$, and $q_{u,i}$ are set at the 90th, 80th, and 99th percentiles of each margin, respectively, with $s_{u,i} = 10$ in [\(13\)](#). Parameters in [\(14\)](#) are specified as $u_a = u_\sigma = 50, l_\gamma = -1$, and $u_\gamma = 1$.

For the sampling process, we employ a random-walk sampler to derive 3,000 posterior samples from three parallelly executed chains, each comprising 30,000 iterations with a burn-in of 20,000 and a thinning rate of 10. Each scenario is replicated 1000 times to accommodate the variability inherent in the data generation phase. Outcomes, including the average posterior mean, average 95% credible interval (CI) length, and coverage rates for these CIs, are reported in [Tables 1 and 2](#). As we expected, the coverage rate for the true values closely approximates 0.95 across all parameters and scenarios.

	Scenario 1.1			Scenario 1.2			Scenario 1.3		
	TV	EST	CR	TV	EST	CR	TV	EST	CR
a_1	0.5	0.55 (0.52)	0.95	0.5	0.54 (0.47)	0.95	0.5	0.53 (0.45)	0.94
a_2	1.2	1.23 (0.86)	0.95	1.2	1.25 (0.83)	0.96	1.2	1.25 (0.82)	0.96
σ_1	0.5	0.52 (0.3)	0.95	0.5	0.51 (0.29)	0.94	0.5	0.51 (0.28)	0.95
σ_2	1.2	1.25 (0.66)	0.95	1.2	1.23 (0.64)	0.96	1.2	1.23 (0.64)	0.95
γ_1	0.3	0.31 (0.4)	0.96	0.2	0.22 (0.39)	0.95	-0.1	-0.09 (0.35)	0.95
γ_2	0.1	0.09 (0.25)	0.95	-0.2	-0.2 (0.3)	0.96	-0.3	-0.3 (0.32)	0.95
u_1	5.5	5.51 (0.21)	0.95	5.5	5.5 (0.14)	0.94	5.5	5.5 (0.12)	0.95
u_2	6.7	6.7 (0.08)	0.94	6.7	6.7 (0.08)	0.95	6.7	6.7 (0.09)	0.95

Table 1: Estimation outcomes for tail parameters and thresholds across three distinct scenarios. The column TV specifies the true values, whereas the EST enumerates the mean posterior means and mean lengths of the 95% credible intervals (denoted within brackets) derived from 1000 repetitive trials. The last column CR documents the coverage rates achieved by these credible intervals.

	Scenario 1.1			Scenario 1.2			Scenario 1.3		
	TV	EST	CR	TV	EST	CR	TV	EST	CR
$U[1, 2]$	0.7	0.7 (0.05)	0.96	0.7	0.7 (0.05)	0.96	0.7	0.7 (0.05)	0.96
$U[2, 2]$	0.714	0.71 (0.05)	0.96	0.714	0.71 (0.05)	0.96	0.714	0.71 (0.05)	0.96
μ_1	3.5	3.5 (0.09)	0.97	3.5	3.5 (0.09)	0.98	3.5	3.5 (0.09)	0.98
μ_2	4	4 (0.13)	0.98	4	4 (0.13)	0.98	4	4 (0.13)	0.98
s_1	1	1 (0.07)	0.97	1	1 (0.07)	0.96	1	1 (0.07)	0.96
s_2	1.5	1.5 (0.1)	0.97	1.5	1.5 (0.1)	0.98	1.5	1.5 (0.1)	0.98

Table 2: Continued table for estimation outcomes for the bulk parameters. $U[1, 2]$ and $U[2, 2]$ are the (1,2) and (2,2) elements of the Cholesky factor of the correlation matrix, respectively.

We also assess our model's performance under misspecification, in particular, we evaluate the models' ability to discern data dependencies accurately. In scenario 2, we exclusively generate data points from a bivariate normal distribution. The true parameters remain consistent with those in Table 2. For a random pair (X_1, X_2) and its independent replicate (X'_1, X'_2) with marginal distribution F_1 and F_2 , the overall dependence is evaluated by Kendall's rank coefficient $\tau = 2\mathbb{P}((X_1 - X'_1)(X_2 - X'_2) > 0)$. Pairwise tail or asymptotic dependence is measured by the tail dependence coefficient χ , defined as

$$\chi(r) = \frac{\mathbb{P}(F_1(X_1) > r, F_2(X_2) > r)}{1 - r}, \quad 0 < r < 1.$$

The limit of $\chi(r)$ as r approach 1, referred to as χ , conveys information about asymptotic dependence. A bivariate distribution exhibits asymptotic independence if $\chi = 0$ and asymptotic dependence otherwise. The theoretical χ for our model can be expressed analytically as follows. For $r > \max\{F_1(u_1), F_2(u_2)\}$,

$$\begin{aligned} \mathbb{P}(F_i(X_i) > r) &= \mathbb{P}(F_{\text{bulk}}(u_1, u_2) + [1 - F_{\text{bulk}}(u_1, u_2)]H_i(X_i - u_i) > r) \\ &= \mathbb{P}\left(H_i(X_i - u_i) > \frac{r - F_{\text{bulk}}(u_1, u_2)}{1 - F_{\text{bulk}}(u_1, u_2)}\right), \end{aligned}$$

where H_i is the marginal distribution of the mGPD in (9). Let $r^* = [r - F_{\text{bulk}}(u_1, u_2)]/[1 - F_{\text{bulk}}(u_1, u_2)]$. Then

$$\begin{aligned} \chi &= \lim_{r^* \rightarrow 1^-} \chi(r^*) = \frac{\mathbb{P}(H_1(X_1 - u_1) > r^*, H_2(X_2 - u_2) > r^*)}{1 - r^*} \\ &= 1 - \left(\frac{1 + a_{(1)}}{1 + a_{(2)}}\right)^{1+a_{(2)}^{-1}} \frac{a_{(2)}}{a_{(1)}} \frac{a_1 a_2}{a_1 a_2 + a_1 + a_2}, \end{aligned}$$

where $a_{(1)} = \min\{a_1, a_2\}$, $a_{(2)} = \max\{a_1, a_2\}$. This final equation is derived from the χ of the mGPD, as discussed in Kiriliouk et al. (2019). Since χ is positive for all positive a_1 and a_2 , our model exhibits asymptotic dependence.

While $\chi(r)$ is effective for distributions with asymptotic dependence, it offers limited insights for asymptotically independent distributions, such as a bivariate normal distribution with correlation $\rho < 1$ (Sibuya, 1960). To achieve a comprehensive evaluation, we also compute

$$\bar{\chi}(r) = \frac{2 \log \mathbb{P}(F_1(X_1) > r)}{\log \mathbb{P}(F_1(X_1) > r), F_2(X_2) > r)} - 1,$$

defined by Coles et al. (1999). This metric specifically quantifies distinctions within the class of asymptotically independent distributions. Analogous to $\chi(r)$, the value $\bar{\chi} = \lim_{r \rightarrow 1^-} \bar{\chi}(r)$

indicates the strength of extremal dependence. For an asymptotic independent distribution, $\bar{\chi}$ falls within the range $[-1, 1)$, and $\bar{\chi}$ increases with the strength of extremal dependence and goes to 1 for asymptotically dependent distributions.

The bivariate version of our multivariate extreme mixture model (which will be denoted as BEMM) is set against the model presented by [André et al. \(2024\)](#), which focuses on smoothly combining two copulae tailored to the bulk and tail. This approach, henceforth referred to as bivariate mixture copula model (BMCM), has the smallest AIC on bivariate normally distributed data when it employs a Student’s t copula for the bulk and an inverted Gumbel copula for the tail, according to André’s experiments. Our evaluation benchmarks the performance of BEMM against this optimal configuration of BMCM.

To ensure a fair comparison with the frequentist inferences drawn from BMCM, we average the empirical dependence metrics estimated from 3000 replicated datasets, each comprising 2000 data points, as a singular point of estimation in each simulation. These replicated datasets, denoted as y_{rep} are generated from the distribution

$$p(\mathbf{y}_{rep}|\mathbf{X}) = \int p(\mathbf{y}|\boldsymbol{\theta})p(\boldsymbol{\theta}|\mathbf{X})d\boldsymbol{\theta}, \quad (16)$$

where $p(\mathbf{y}|\boldsymbol{\theta})$ represents BEMM’s data-generating distribution and $p(\boldsymbol{\theta}|\mathbf{X})$ is the posterior distribution.

Figure 2 displays boxplots of $\chi(r)$, $\bar{\chi}(r)$ and Kendall’s τ calculated from 100 repeated simulations of BMCM and 1000 of BEMM. Here, the number of BMCM simulations aligns with those in André’s paper. Due to parameter uncertainty in Bayesian inference, we have expanded the BEMM simulations to 1000. In assessing extremal dependence, both models exhibit similar performance for $r \leq 0.95$. However, at $r = 0.99$, our BEMM tends to slightly overestimate $\chi(r)$ and $\bar{\chi}(r)$, contrary to BMCM’s underestimated results. Notably, the true values are inclusively captured within the span of the boxes for all thresholds. Regarding Kendall’s τ , the differences between the two models are negligible. Conclusively, even when faced with model misspecification, our BEMM demonstrates commendably accurate and competitive performance.

5 Applications

Over the last decade, the UK has experienced a significant rise in heatwave occurrences. In 2022, the air temperature soared to a record-breaking 40.3° C. This prolonged period of intense

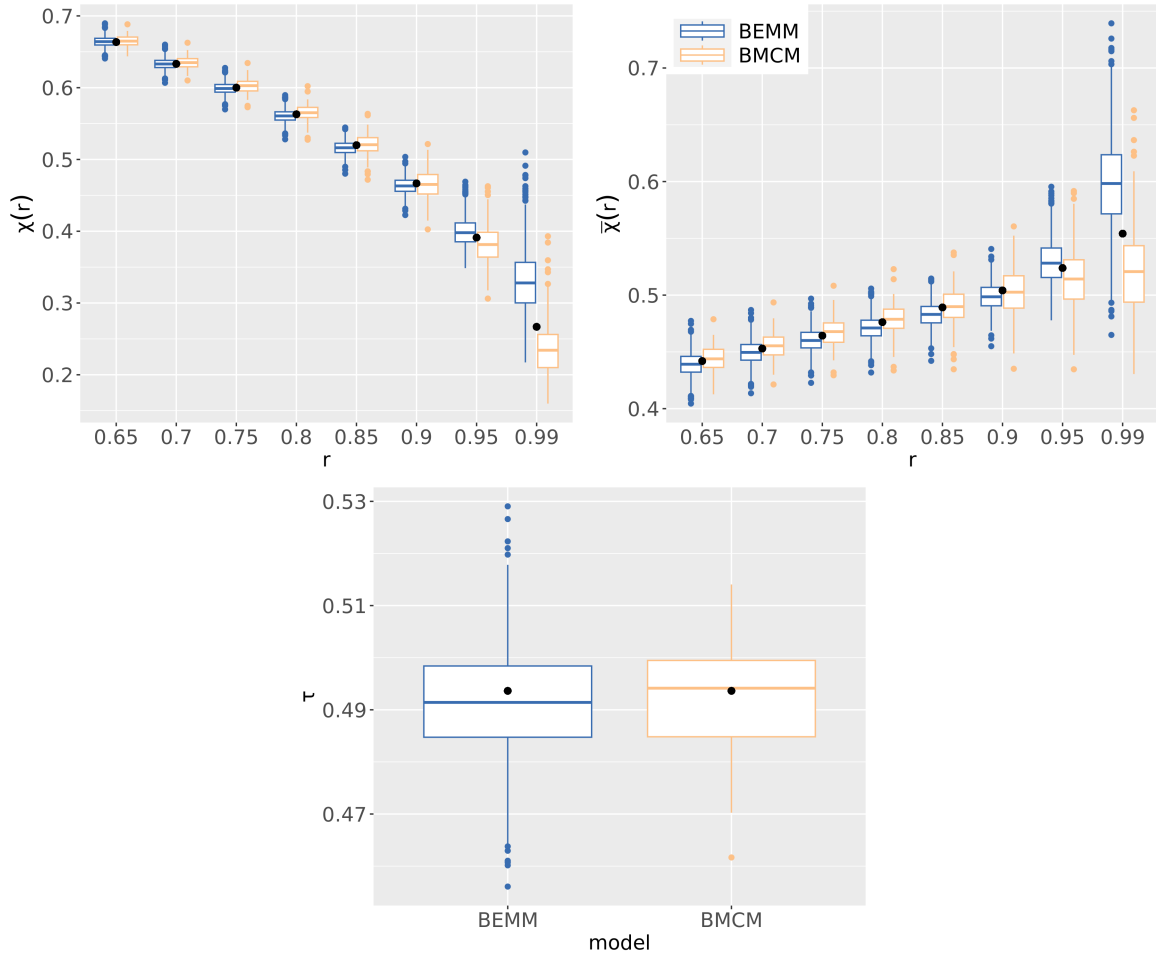


Figure 2: Boxplots of $\chi(r)$, $\bar{\chi}(r)$ and Kendall's τ in the scenario 2. The yellow boxes denote empirical metrics derived from predictions from 100 simulations, whereas the blue boxes represent the averaged empirical metrics computed from 3000 replicated data in 1000 simulations. The black points signify the true value for each dependence metric.

heat has been linked to an estimated 3,000 fatalities and has caused substantial delays and cancellations in train services and flights. To investigate the behavior of daily air temperatures during such extraordinary weather events and to analyze the comparative temperature patterns of two regions, we study the daily maximum air temperatures recorded at two sites: one station in Bishop’s Lane, Ringmer, East Sussex, and the other one in Model Farm, Shirburn, Oxfordshire. The data for this study are publicly available from the Center for Environmental Data Analysis ([CEDA](#)). The most recent archived records of air temperature at the time of our research extend up to July 2022, and we focus on the most recent six-year period from 2016 to 2021. After excluding entries with missing values, 1,945 daily maximum temperature records remain for analysis.

Daily air temperatures exhibit pronounced seasonality and autocorrelation; the temperature on any given day is heavily influenced by the temperature of the preceding day and the time of year. To account for these factors, we employ sinusoidal functions of time to capture seasonal variations and a lag-1 autoregressive term to model the dependence between temperatures on successive days. Specifically, for the air temperature $Y_{t,j}$ on day t at site $j = 1, 2$, we assume

$$Y_{t,j} = \beta_{0,j} + \beta_{1,j} \sin\left(\frac{2\pi}{365}t\right) + \beta_{2,j} \cos\left(\frac{2\pi}{365}t\right) + \beta_{3,j}Y_{t-1,j} + \varepsilon_j, \quad (17)$$

where $\beta_{i,j}, i = 1, 2, 3$ are linear coefficients and ε_j represents the noise term. We verify the stationarity of the residuals through autocorrelation plots (not shown here). The joint negative residual $\mathbf{E} = -(\varepsilon_1, \varepsilon_2)$, as shown in Figure 3, present elongated right tails for both margins and strong extreme dependence. To comprehensively characterize these joint residuals, we apply our BEMM model to \mathbf{E} with the same priors used for simulation. This is because the negative residuals display similar behavior to the simulated data in scenarios 1.1-1.3 in Section 4. Additionally, we include the constraints $\gamma_i + 1/a_i \geq 0, i = 1, 2$ to ensure finite expectation, facilitating the predictive accuracy evaluation at the end of this section. We executed three parallel AFSS samplers, each running for 20000 iterations. The initial 10000 iterations were discarded as burn-in period, after which the samples were thinned by selecting every 10th sample. Convergence is diagnosed by checking trace plots and monitoring the Gelman-Rubin diagnostic. Figure 4 displays the histograms of posterior samples for all parameters. Notably, the histograms for u_1 and u_2 exhibit a multimodal pattern. For u_1 , the most prominent mode is near 3.2, aligning with the 92nd percentile, while two smaller peaks at 2.7 and 3.6 correspond to the 89th and 94th percentiles, respectively. In contrast, u_2 ’s histogram is left-skewed, with

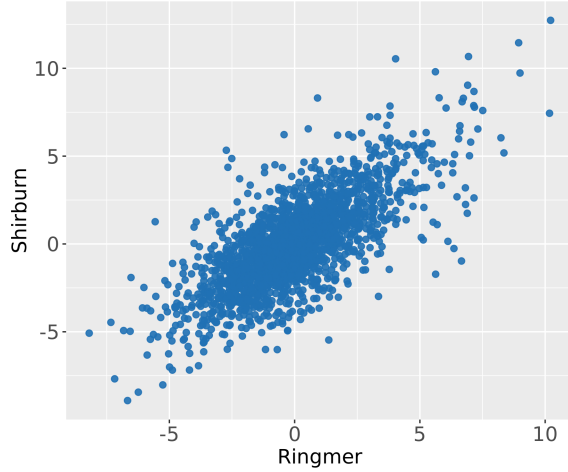


Figure 3: Scatterplot of the negative residuals from model (17).

concentrations around 3.7, 4.0, and 4.3, matching the 93rd, 94th, and 95th percentiles. This suggests the presence of multiple plausible values for the threshold. Note that this uncertainty is completely ignored by setting a fixed threshold in the standard threshold-exceedance modeling.

Model evaluation is conducted via posterior predictive checks, emphasizing the analysis of both marginal quantiles and dependence measures. By generating 3000 replications of \mathbf{E} using 16, we establish posterior predictive distributions of marginal quantiles, $\chi(r)$, $\bar{\chi}(r)$, and Kendall's τ . Figure 5 contrasts the posterior predictive quantile derived from the replicated data with the empirical quantile of \mathbf{E} , plotted across uniformly distributed percentiles ranging from 0 to 0.99. For each empirical quantile, the corresponding mean of the prediction closely aligns with the 45-degree line, which is also situated within the 95% credible band of the predicted quantile. We also include quantiles from an estimated bivariate normal distribution based on \mathbf{E} by the maximum likelihood approach. It is clear from the results that our BEMM outperforms the bivariate normal model, particularly in accurately estimating higher quantiles on both margins.

Figure 6 depicts the posterior predictions of $\chi(r)$, $\bar{\chi}(r)$, and Kendall's τ , alongside their respective empirical values. The 95% credible interval of the theoretical χ is included for the $\chi(r)$ plot. For both $\chi(r)$ and $\bar{\chi}(r)$, the empirical measurements reside within the 95% credible band across all values of r , with the sole exception at 0.68. Notably, the theoretical χ lies in the central region of the 95% credible band of the posterior predictive $\chi(r)$. As r approaches 1,

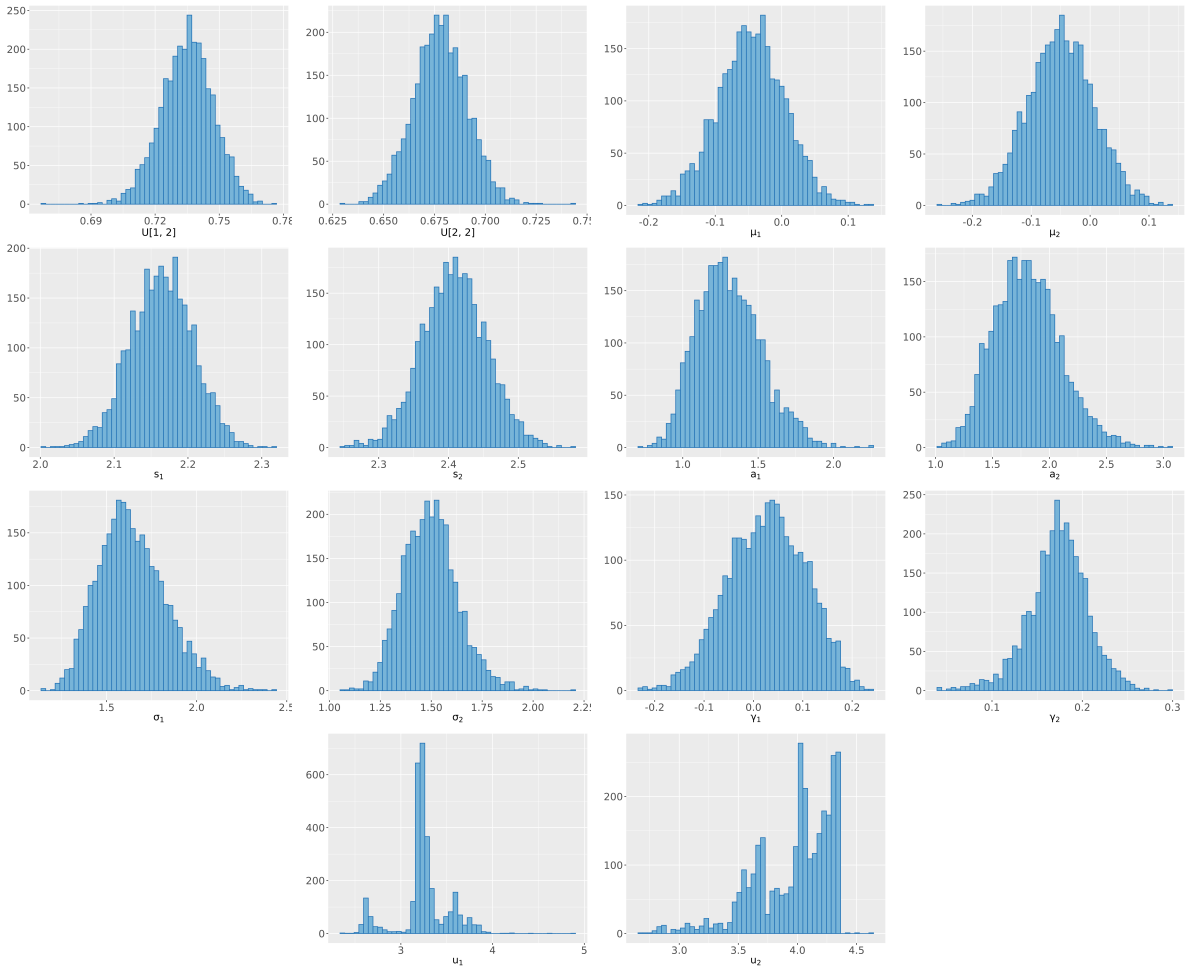


Figure 4: Histograms of the posterior distribution for each parameter of our model. The first six plots align with those parameters presented in Table 2, while the subsequent plots showcase parameters from Table 1. The histograms of the threshold parameters u_1, u_2 exhibit distinct multimodality, contrasting sharply with the bell-shaped distributions observed in the histograms of the remaining parameters.

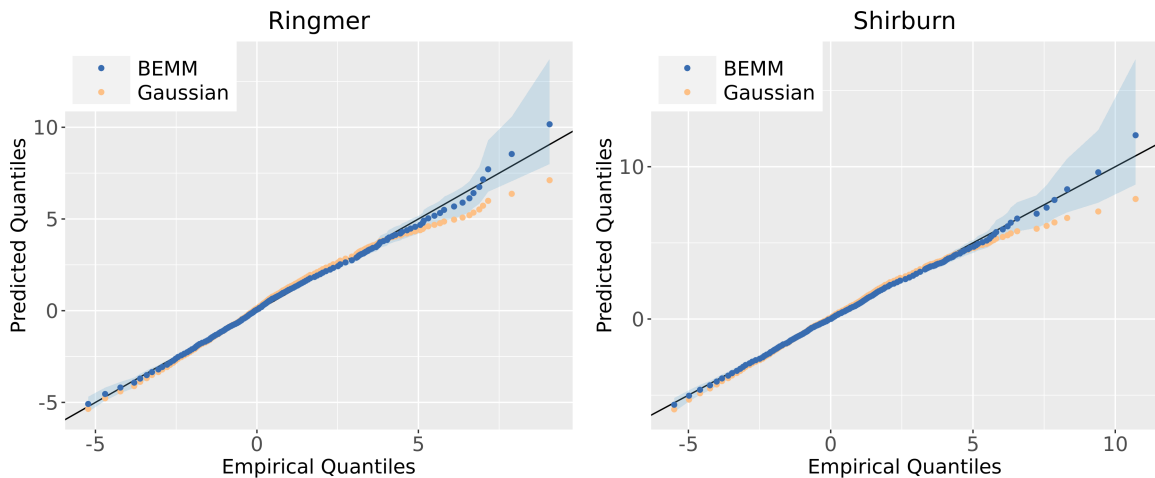


Figure 5: Quantile-quantile plot of the posterior predictive mean from 3000 replicate data sets (in blue) against the empirical quantile. The shaded area is the 95% credible band. Quantiles of an estimated bivariate normal distribution using the maximum likelihood method are included (in orange).

the empirical $\chi(r)$ falls in the tail region of the theoretical χ distribution, while empirical $\bar{\chi}(r)$ moves towards the posterior mean. Additionally, the empirical value of Kendall’s τ aligns closely with the mode of the posterior predictive distribution, suggesting an effective fit concerning the underlying dependence structure.

The final segment of our analysis quantifies the predictive accuracy of our BEMM in comparison to the Gaussian model, utilizing the energy score, which is a multivariate extension of the continuous rank probability score, as detailed by [Gneiting and Raftery \(2007\)](#). The energy score is a scoring rule that quantifies the divergence between an observed value, y , and a forecasted distribution F according to

$$\text{ES}(F, \mathbf{y}) = \mathbb{E}_F \|\mathbf{X} - \mathbf{y}\| - \frac{1}{2} \mathbb{E}_F \|\mathbf{X} - \mathbf{X}'\|, \quad (18)$$

where \mathbf{X} and \mathbf{X}' independently follow F , and $\|\cdot\|$ denotes the Euclidean norm. This metric integrates the expected value of the Euclidean distance between forecasted and actual observations while accounting for the dispersion within the forecasted values themselves. It is proper, provided F has finite expectation.

For instances where specific forecasting aspects are prioritized, such as extreme event prediction, the concept of a weighted energy score becomes pertinent. Two common frameworks for this adjusted metric include the outcome-weighted energy score and the threshold-weighted

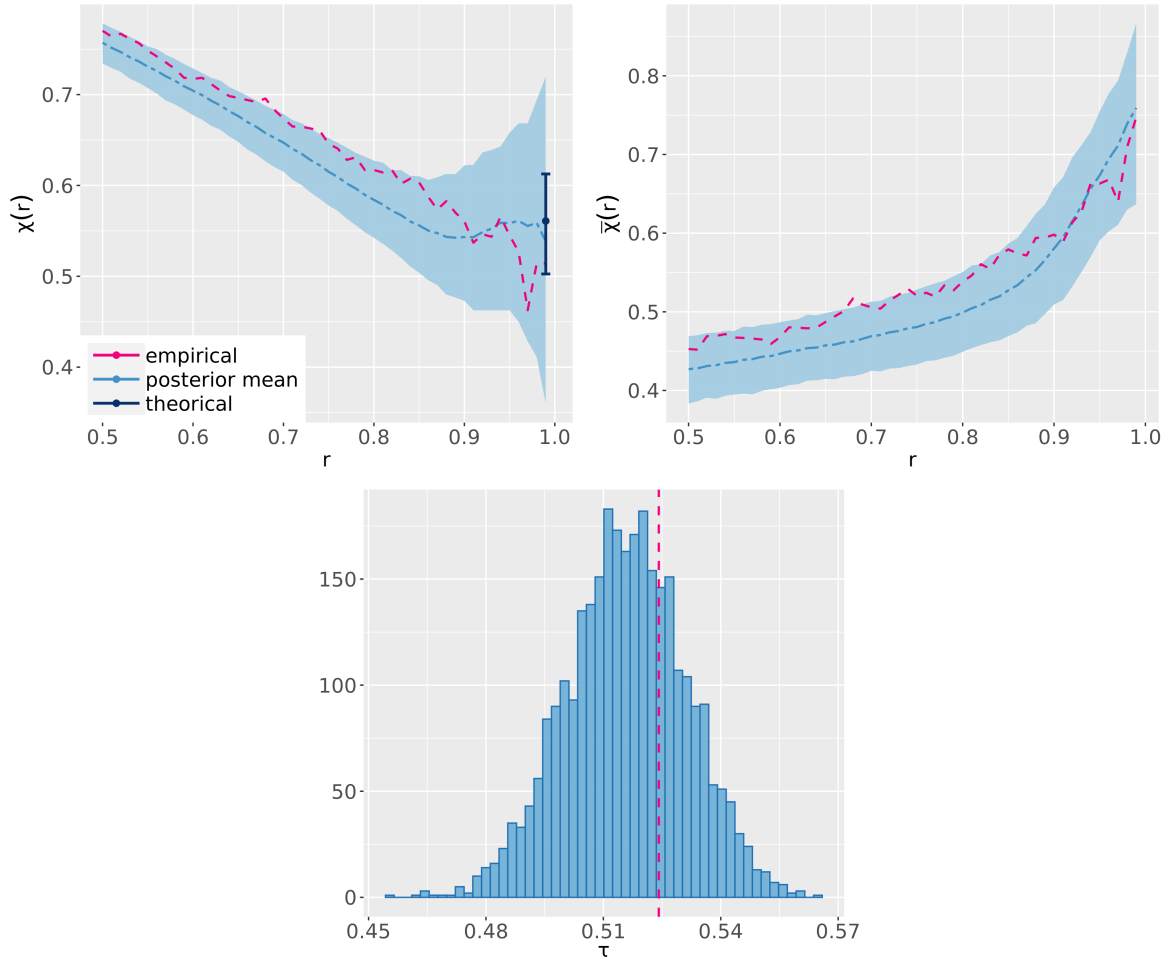


Figure 6: Based on 3000 replicate from the posterior predictive distribution, the upper two plots present empirical values vs. means of the posterior prediction, each accompanied by a 95% credible band, of $\chi(r)$ and $\bar{\chi}(r)$. The error bar in the $\chi(r)$ plot represents the 95% credible interval of the theoretical χ , with the center point indicating the posterior mean. The lower plot features a histogram of the posterior predictive Kendall's τ , with the empirical value highlighted in red.

energy score (Holzmann and Klar, 2017; Allen et al., 2023). The outcome-weighted variant applies a weighting function, $w(\cdot) : \mathbb{R}^d \rightarrow [0, 1]$ directly to the observations and forecast points within a specified region of interest. Conversely, the threshold-weighted version employs a chain function $v : \mathbb{R}^d \rightarrow \mathbb{R}^d$ derived from $w(\cdot)$ on the vectors before they are assessed using the energy score equation. Our analysis employs two distinct weighting strategies within these frameworks. The first, W_1 , targets only the area where all elements exceed the marginal 90th percentiles, Q_1 and Q_2 , from the fitted data \mathbf{E} . In contrast, W_2 adopts a smoother weighting to highlight the tail region of the distribution. This methodology uses the weight from the cdf of a bivariate normal distribution, incorporating the sample mean $\hat{\boldsymbol{\mu}}$ and covariance matrix $\hat{\boldsymbol{\Sigma}}$ of \mathbf{E} .

Table 3 presents a detailed comparison of the energy scores, including the outcome-weighted and threshold-weighted variants, for both our BEMM and the Gaussian model, employing the previously described weighting strategies. Significantly, across all categories, our BEMM invariably reports lower scores, indicating superior performance.

	W_1			W_2	
	ES	OWES	TWES	OWES	TWES
BEMM	2.0155	0.0830	0.2512	0.5546	1.0361
Gaussian	2.0197	0.0896	0.2517	0.5567	1.0384

Table 3: Energy Score (ES), outcome-weighted energy score (OWES), and threshold-weighted energy score (TWES) of BEMM and Gaussian model. W_1 assigns weights exclusively within region where all components surpass the 90th percentile of \mathbf{E} , while W_2 uses the cdf of the MVN($\hat{\boldsymbol{\mu}}, \hat{\boldsymbol{\Sigma}}$) as weighting function. Here, $\hat{\boldsymbol{\mu}}$ and $\hat{\boldsymbol{\Sigma}}$ represent the sample mean and covariance matrix of \mathbf{E} , respectively.

6 Discussion and conclusion

We proposed a Bayesian multivariate extreme value mixture model to capture bulk and extreme values accurately. Our method treats the typically problematic aspect of threshold selection in peaks over threshold models by integrating the threshold as a parameter within our framework. Although here we use the multivariate Gaussian distribution to describe the bulk, our general

construction in (11) allows the selection by the user of virtually any parametric model, as long as it belongs to the MDA of an mGEVD. Our simulation studies for the bivariate case reveal that our model excels in handling a variety of tail behaviors when properly configured and remains competitive in estimation accuracy compared to alternative bivariate methods, even when the model is misspecified. Our application to UK daily maximum air temperatures shows that our model notably enhances the precision of tail estimations compared to a standard Gaussian approach. Furthermore, our model demonstrates a precise grasp of both the central and extremal dependence structures.

Our modeling approach and tailored Bayesian inference proposed in Section 3 are easily described in the general $d \geq 2$ dimensional setting. Unfortunately, computational limitations stemming from our model make scalability cumbersome. A natural way to overcome these limitations is through pairwise likelihood, a case of composite likelihood techniques that uses the likelihood of pairs instead of the full likelihood. The composite marginal likelihood for Bayesian inference has been used and discussed in [Pauli et al. \(2011\)](#), and its applicability to max-stable processes for spatial extremes has been explored by, e.g., [Smith and Stephenson \(2009\)](#) and [Ribatet et al. \(2012\)](#). See also [Chan and So \(2017\)](#) for a discussion of the performance of Bayesian composite likelihood estimation of max-stable processes. Replacing the full likelihood of our model with its pairwise composite counterpart leads to a proper posterior distribution. However, adjustments might be needed since this posterior distribution can differ from the one obtained by the full likelihood (see, e.g., the adjustments proposed by [Ribatet et al., 2012](#)).

Our approach could face potential challenges when data displays a pronounced light tail, i.e., when $\gamma_i < 0$. In such a scenario, the bivariate GPD presents an upper boundary yet lacks a lower one. This absence can lead to a discrepancy between the scales of the marginal mGPD and the bulk distribution, resulting in an unintended marginal distribution where its left tail is dominated by the marginal mGPD. To mitigate this issue, a truncated bivariate GPD, which sets a lower threshold, can provide a more accurate representation of the actual data.

Acknowledgements

We thank Lidia Andre (Lancaster University) for facilitating the code to implement the bivariate mixture copula model.

Supplementary material

Code to fit the bivariate version of our extreme mixture model and reproduce the data application in Section 5 is freely available at https://github.com/hcl1516926907/Biv_Ext_Mix_Mod.

Appendix

We introduce the following Lemmas to facilitate the proof of Proposition 1

Lemma 1. *The mGPD $H(\mathbf{x})$ in (4) is in the MDA of the mGEVD $G(\mathbf{x})$.*

Proof. Theorem 2.2 in Rootzén and Tajvidi (2006) states that if \mathbf{X} follows an mGPD $H(\mathbf{x})$ defined in (4), then there exists an increasing curve $\mathbf{u}(t)$ with $P(\mathbf{X} \leq \mathbf{u}(t)) \rightarrow 1$ as $t \rightarrow \infty$ and a function $\boldsymbol{\sigma}(\mathbf{u}) > \mathbf{0}$ such that

$$\mathbb{P} \left(\frac{\mathbf{X} - \mathbf{u}(t)}{\boldsymbol{\sigma}(\mathbf{u}(t))} \leq \mathbf{x} \mid \frac{\mathbf{X} - \mathbf{u}(t)}{\boldsymbol{\sigma}(\mathbf{u}(t))} \not\leq \mathbf{0} \right) = H(\mathbf{x}).$$

Following Theorem 2.1(ii) in the same paper, $H(\mathbf{x})$ is in the MDA of $G(\mathbf{x})$. □

Lemma 2. *Suppose the univariate distribution $F_1(x)$ and $F_2(x)$ have the same right endpoint $x^* = \sup\{F_i(x) < 1\}, i = 1, 2$. If F_1 and F_2 are in the MDA of G_1 and G_2 , respectively, then the mixture distribution $F_{\text{mix}}(x) = pF_1(x) + (1-p)F_2(x), 0 < p < 1$ is in the MDA of some GEVD G_{mix} .*

Proof. Define $l =: \lim_{x \rightarrow x^*-} [1 - F_1(x)]/[1 - F_2(x)]$. Possible values of l are 0, $+\infty$ or some constant $\alpha > 0$. As established by Theorem 2.9 in Praveena et al. (2019), F_{mix} falls within the MDA of G_2 when $l = 0$. Conversely, if $l = +\infty$, F_{mix} is in the MDA of G_1 . In the case $l = \alpha$, notice that $\lim_{x \rightarrow x^*-} [1 - F_{\text{mix}}(x)]/[1 - F_2(x)] = \{p[1 - F_1(x)] + (1-p)[1 - F_2(x)]\}/[1 - F_2(x)] = p\alpha + 1 - p$ is a positive constant. According to Theorem 2.1 in Resnick (1971), F_{mix} is in the MDA of $G_2^{p\alpha+1-p}$. □

Remark. *When $l = \alpha$, $F_1(x)$ and $F_2(x)$ are called tail equivalent, and we have $G_2^\alpha(x) = G_1(x)$.*

Proof of Proposition 1. We complete the proof by considering three cases.

1. When no components exceed the threshold, the distribution F is degenerated to

$$F(\mathbf{x}) = \begin{cases} F_{\text{bulk}}(\mathbf{x}), & \mathbf{x} \leq \mathbf{u}, \\ 1, & \text{otherwise.} \end{cases} \quad (19)$$

If F is in the MDA of an mGEVD with non-degenerated margins, by definition, there exist $\mathbf{a}_n \in (0, \infty)^d$, $\mathbf{b}_n \in \mathbb{R}^d$, such that

$$\lim_{n \rightarrow \infty} F^n(\mathbf{a}_n \mathbf{x} + \mathbf{b}_n) = G(\mathbf{x}).$$

For any \mathbf{x} that satisfies $\mathbf{a}_n \mathbf{x} + \mathbf{b}_n \leq \mathbf{u}$, (19) implies

$$\lim_{n \rightarrow \infty} F^n(\mathbf{a}_n \mathbf{x} + \mathbf{b}_n) \leq \lim_{n \rightarrow \infty} F_{\text{bulk}}^n(\mathbf{u}) = 0,$$

due to the fact that $0 < F_{\text{bulk}}^n(\mathbf{u}) < 1$. Conversely, for those \mathbf{x} that do not satisfy $\mathbf{a}_n \mathbf{x} + \mathbf{b}_n \leq \mathbf{u}$, we have

$$\lim_{n \rightarrow \infty} F^n(\mathbf{a}_n \mathbf{x} + \mathbf{b}_n) = 1$$

However, these two equations present a contradiction with the non-degeneracy condition of $G(\mathbf{x})$.

2. When all components exceed the threshold, we have

$$F(\mathbf{x}) = F_{\text{bulk}}(\mathbf{u}) + [1 - F_{\text{bulk}}(\mathbf{u})]H_U(\mathbf{x} - \mathbf{u}),$$

for any $\mathbf{x} > \mathbf{u}$. Let $\mathbf{x}_F^* = (x_1^*, \dots, x_d^*)$, where $x_i^* = \sup\{F_i(x) < 1\}$ is the upper bound of margin i . Then,

$$\begin{aligned} \lim_{\mathbf{x} \rightarrow \mathbf{x}_F^{*-}} &= \frac{1 - H_U(\mathbf{x} - \mathbf{u})}{1 - F(\mathbf{x})} \\ &= \frac{1 - H_U(\mathbf{x} - \mathbf{u})}{1 - F_{\text{bulk}}(\mathbf{u}) - [1 - F_{\text{bulk}}(\mathbf{u})]H_U(\mathbf{x} - \mathbf{u})} \\ &= \frac{1}{1 - F_{\text{bulk}}(\mathbf{u})} > 0. \end{aligned}$$

By Lemma 1, there exist a sequence of vector $\mathbf{a}_n > \mathbf{0}$ and \mathbf{b}_n such that $H_U^n(\mathbf{a}_n(\mathbf{x} - \mathbf{u}) + \mathbf{b}_n) \rightarrow G(\mathbf{x})$. Following the proof to Theorem 2.1 in Resnick (1971), the above implies that $F^n(\mathbf{a}_n \mathbf{x} + \mathbf{b}_n - \mathbf{a}_n \mathbf{u}) \rightarrow G^{1-F_{\text{bulk}}(\mathbf{u})}(\mathbf{x})$, where $G^{1-F_{\text{bulk}}(\mathbf{u})}(\mathbf{x})$ is also an mGPD by the max-stable property of an mGPD.

3. When some components exceed the threshold while others do not, we simplify the proof by considering the bivariate case for ease of exposition. The extension to the multivariate case is straightforward.

A necessary and sufficient condition for $F(x_1, x_2)$ to be in the MDA of an mGEVD $\Phi(x_1, x_2)$ (Beirlant, 2004, p. 281) is that the margins $F_i(x_i)$ are in the MDA of the marginal distributions $\Phi_i(x_i)$, $i = 1, 2$ and the copula of F defined as $C_F(w_1, w_2) = F\{F_1^{-1}(w_1), F_2^{-1}(w_2)\}$, $(w_1, w_2) \in [0, 1]^2$ satisfies

$$\lim_{n \rightarrow \infty} C_F^n(w_1^{1/n}, w_2^{1/n}) = C_\Phi(w_1, w_2), \quad (20)$$

where $C_\Phi(w_1, w_2)$ is the copula of $\Phi(x_1, x_2)$. Equivalently, (20) can be expressed as

$$\lim_{n \rightarrow \infty} n \left[1 - C_F\left(1 - \frac{v_1}{n}, 1 - \frac{v_2}{n}\right) \right] = -\log C_\Phi(\exp(-v_1), \exp(-v_2)), \quad v_1, v_2 \geq 0 \quad (21)$$

by taking logarithms and a linear expansion (see, e.g., Segers 2012). The term $-\log C_\Phi(\exp(-v_1), \exp(-v_2))$ is known as the stable tail dependence function (Segers, 2012). We proceed with the proof by showing both the margins satisfy the above conditions while the copula does not.

For $x_1 \leq u_1, x_2 \leq u_2$, define the (cumulative distribution) functions $B(x_1, x_2)$, $B_1(x_1)$ and $B_2(x_2)$ as

$$\begin{aligned} B(x_1, x_2) &= \frac{F_{\text{bulk}}(x_1, x_2)}{F_{\text{bulk}}(u_1, u_2)}, \\ B_1(x_1) = B(x_1, u_2) &= \frac{F_{\text{bulk}}(x_1, u_2)}{F_{\text{bulk}}(u_1, u_2)}, \\ B_2(x_2) = B(u_1, x_2) &= \frac{F_{\text{bulk}}(u_1, x_2)}{F_{\text{bulk}}(u_1, u_2)}. \end{aligned}$$

A straightforward application of Theorem 1.1.8 in de Haan and Ferreira (2006, p. 17) implies that $B_1(x)$ and $B_2(x)$ are in the MDA of Weibull-type GPDs $\psi_{1,\gamma}, \psi_{2,\gamma}$ with shape parameter $\gamma = -1$. Also, we use $H_1(x_1) = H_U(x_1, \eta_2^u), x_1 \in [\eta_1^l, \eta_1^u]$, $H_2(x_2) = H_U(\eta_1^u, x_2), x_2 \in [\eta_2^l, \eta_2^u]$ to denote the marginal distributions of $H_U(x_1, x_2)$. Since $H_U(\mathbf{x})$ is in the MDA of $G(\mathbf{x})$ by Lemma 1, $H_1(x_1)$ and $H_2(x_2)$ are also in the MDA of $G(x_1), G(x_2)$ by marginalizing (1).

Assuming only the first component exceeds the threshold, the situation is depicted in Figure 7. This implies $\eta_1^l = 0, \eta_2^u = 0$. Specifically, when $x_1 \geq u_1$, we have:

$$\begin{aligned} F_1(x_1) &= \int_{\min\{-\infty, u_1 + \eta_1^l\}}^{x_1} \int_{\min\{-\infty, u_2 + \eta_2^l\}}^{\max\{u_2, u_2 + \eta_2^u\}} f(x_1, x_2) dx_2 dx_1 \\ &= \int_{-\infty}^{u_1} \int_{-\infty}^{u_2} f(x_1, x_2) dx_2 dx_1 + \int_{u_1 + \eta_1^l}^{x_1} \int_{u_2 + \eta_2^l}^{u_2 + \eta_2^u} f(x_1, x_2) dx_2 dx_1 \\ &= F_{\text{bulk}}(u_1, u_2) + [1 - F_{\text{bulk}}(u_1, u_2)] H_1(x_1 - u_1), \end{aligned}$$

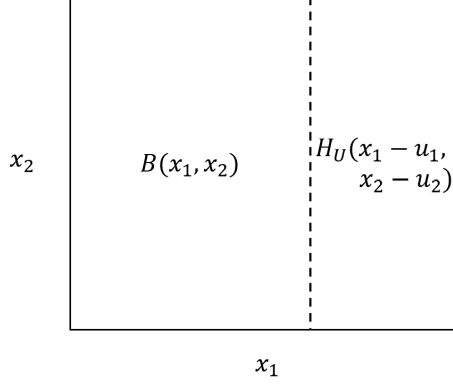


Figure 7: Demonstration of the situation where x_1 exceeds the threshold but x_2 does not. The square represents the \mathbb{R}^2 space, and the dashed line indicates the threshold. The right-hand side region of the threshold is completely determined by $H_U(x_1 - u_1, x_2 - u_2)$, which is a bivariate GPD with $x_1 \geq u_1, x_2 < u_2$

Since $\lim_{x_1 \rightarrow \infty} [1 - H_1(x_1 - u_1)]/[1 - F_1(x_1)] = 1/(1 - F_{\text{bulk}}(u_1, u_2))$, we conclude that $F_1(x_1)$ is in the MDA of $G_1^{1-F_{\text{bulk}}(u_1, u_2)}$ by Theorem 2.1 in [Resnick \(1971\)](#). Similarly, the marginal distribution for the second component (which does not exceed the threshold) is

$$\begin{aligned}
F_2(x_2) &= \int_{\min\{-\infty, u_1 + \eta_1^l\}}^{\max\{u_1, u_1 + \eta_1^u\}} \int_{\min\{-\infty, u_2 + \eta_2^l\}}^{x_2} f(x_1, x_2) dx_2 dx_1 \\
&= \int_{-\infty}^{u_1} \int_{-\infty}^{x_2} f(x_1, x_2) dx_2 dx_1 + \int_{u_1 + \eta_1^l}^{u_1 + \eta_1^u} \int_{u_2 + \eta_2^l}^{x_2} f(x_1, x_2) dx_2 dx_1 \\
&= F_{\text{bulk}}(u_1, x_2) + [1 - F_{\text{bulk}}(u_1, u_2)] H_2(x_2 - u_2) \\
&= F_{\text{bulk}}(u_1, u_2) B_2(x_2) + [1 - F_{\text{bulk}}(u_1, u_2)] H_2(x_2 - u_2),
\end{aligned}$$

according to Lemma 2, $F_2(x_2)$ is in the MDA of some GEVD $G_{\text{mix}}(x_2)$.

Next, we demonstrate the existence of $\lim_{n \rightarrow \infty} C_F^n(w_1^{1/n}, w_2^{1/n})$, and show that this limit is not a valid copula.

For any v_1, v_2 in $[0, +\infty)$, we can identify a specific $N = v_1/(1 - F_1(u_1))$ such that $(F_1^{-1}(1 - v_1/n), \cdot)$ falls on the right hand side of the threshold u_1 for all $n > N$. In this

scenario,

$$\begin{aligned}
C_F(w_1, w_2) &= F(F_1^{-1}(w_1), F_2^{-1}(w_2)) \\
&= \int_{\min\{-\infty, u_1 + \eta_1^l\}}^{F_1^{-1}(w_1)} \int_{\min\{-\infty, u_2 + \eta_2^l\}}^{F_2^{-1}(w_2)} f(x_1, x_2) dx_2 dx_1 \\
&= \int_{-\infty}^{u_1} \int_{-\infty}^{F_2^{-1}(w_2)} f(x_1, x_2) dx_2 dx_1 + \int_{u_1 + \eta_1^l}^{F_1^{-1}(w_1)} \int_{u_2 + \eta_2^l}^{F_2^{-1}(w_2)} f(x_1, x_2) dx_2 dx_1 \\
&= F_{\text{bulk}}(u_1, F_2^{-1}(w_2)) + [1 - F_{\text{bulk}}(u_1, u_2)] H_{\mathbf{U}}(F_1^{-1}(w_1) - u_1, F_2^{-1}(w_2) - u_2) \\
&= F_{\text{bulk}}(u_1, u_2) B_2(F_2^{-1}(w_2)) + [1 - F_{\text{bulk}}(u_1, u_2)] H_{\mathbf{U}}(F_1^{-1}(w_1) - u_1, F_2^{-1}(w_2) - u_2).
\end{aligned}$$

Therefore,

$$\begin{aligned}
&\lim_{n \rightarrow \infty} n \left[1 - C_F \left(1 - \frac{v_1}{n}, 1 - \frac{v_2}{n} \right) \right] \\
&= \underbrace{\lim_{n \rightarrow \infty} n F_{\text{bulk}}(u_1, u_2) \left[1 - B_2 \left(F_2^{-1} \left(1 - \frac{v_2}{n} \right) \right) \right]}_{\text{Term 1}} + \\
&\quad \underbrace{\lim_{n \rightarrow \infty} n \left[1 - F_{\text{bulk}}(u_1, u_2) \right] \left[1 - H_{\mathbf{U}} \left(F_1^{-1} \left(1 - \frac{v_1}{n} \right) - u_1, F_2^{-1} \left(1 - \frac{v_2}{n} \right) - u_2 \right) \right]}_{\text{Term 2}}. \tag{22}
\end{aligned}$$

Term 1 is evaluated as follows:

$$\begin{aligned}
\text{Term 1} &= \lim_{n \rightarrow \infty} n F_{\text{bulk}}(u_1, u_2) \left[1 - B_2 \left(F_2^{-1} \left(1 - \frac{v_2}{n} \right) \right) \right] \\
&= F_{\text{bulk}}(u_1, u_2) \lim_{n \rightarrow \infty} n \left[1 - F_2 \left(F_2^{-1} \left(1 - \frac{v_2}{n} \right) \right) \right] \frac{1 - B_2 \left(F_2^{-1} \left(1 - \frac{v_2}{n} \right) \right)}{1 - F_2 \left(F_2^{-1} \left(1 - \frac{v_2}{n} \right) \right)} \\
&= \frac{F_{\text{bulk}}(u_1, u_2)}{F_{\text{bulk}}(u_1, u_2) + [1 - F_{\text{bulk}}(u_1, u_2)] R} v_2 \\
&= -\log \exp \left\{ -\frac{F_{\text{bulk}}(u_1, u_2)}{F_{\text{bulk}}(u_1, u_2) + [1 - F_{\text{bulk}}(u_1, u_2)] R} v_2 \right\},
\end{aligned}$$

where $R = \lim_{x \rightarrow u_2^-} [1 - H_2(x - u_2)] / [1 - B_2(x)]$ can be 0, certain positive value r or ∞ depending on the tail heaviness of H_2 and B_2 (See proof of Lemma 2). The penultimate equation comes from $F_2^{-1}(1 - v_2/n) \rightarrow u_2$ when n goes to infinity.

Before going into Term 2, it is crucial to understand the relationship between the quantile functions $F_i^{-1}(\alpha)$ and $H_i^{-1}(\alpha_i)$, $\alpha_i \in [0, 1]$, $i = 1, 2$. Let x_{F_i} be the α_i -th quantile of $F_i(x)$, i.e. $F_i(x_{F_i}) = \alpha_i$. For margin 1, our interest lies in the case where $x_{F_1} > u_1$. Thus, since $\alpha_1 = F_{\text{bulk}}(u_1, u_2) + [1 - F_{\text{bulk}}(u_1, u_2)] H_1(x_{F_1} - u_1)$, we have

$$x_{F_1} = F_1^{-1}(\alpha_1) = u_1 + H_1^{-1} \left(1 - \frac{1 - \alpha_1}{1 - F_{\text{bulk}}(u_1, u_2)} \right). \tag{23}$$

For margin 2, we lack a similar explicit expression for F_2^{-1} and H_2^{-1} . However, as $\alpha_2 \rightarrow 1^-$, an approximation can be obtained by noting that $\lim_{x_{F_2} \rightarrow u_2^-} [1 - H_2(x_{F_2} - u_2)] / [1 - F_2(x_{F_2})] = R / (F_{\text{bulk}}(u_1, u_2) + [1 - F_{\text{bulk}}(u_1, u_2)]R)$. Hence,

$$x_{F_2} = F_2^{-1}(\alpha_2) \approx u_2 + H_2^{-1} \left(1 - \frac{R(1 - \alpha_2)}{F_{\text{bulk}}(u_1, u_2) + [1 - F_{\text{bulk}}(u_1, u_2)]R} \right). \quad (24)$$

Take (23) and (24) to Term 2, we have

$$\begin{aligned} \text{Term 2} &= [1 - F_{\text{bulk}}(u_1, u_2)] \lim_{n \rightarrow \infty} n \left[1 - H_U \left(H_1^{-1} \left(1 - \frac{v_1^*}{n} \right), H_2^{-1} \left(1 - \frac{v_2^*}{n} \right) \right) \right] \\ &= [1 - F_{\text{bulk}}(u_1, u_2)] \lim_{n \rightarrow \infty} n \left[1 - C_H \left(1 - \frac{v_1^*}{n}, 1 - \frac{v_2^*}{n} \right) \right], \end{aligned}$$

where $v_1^* = v_1 / \{1 - F_{\text{bulk}}(u_1, u_2)\}$, $v_2^* = v_2 R / \{F_{\text{bulk}}(u_1, u_2) + [1 - F_{\text{bulk}}(u_1, u_2)]R\}$, and C_H is the copula of H . Since $H_U(x_1, x_2)$ is in the MDA of some mGEVD $G(x_1, x_2)$, there exists a copula $C_G(w_1, w_2)$ such that

$$\lim_{n \rightarrow \infty} n \left[1 - C_H \left(1 - \frac{w_1}{n}, 1 - \frac{w_2}{n} \right) \right] = -\log C_G(\exp(-w_1), \exp(-w_2)), \quad (25)$$

Consequently, Term 2 converges to the following limit:

$$\text{Term 2} = -[1 - F_{\text{bulk}}(u_1, u_2)] \log C_G(\exp(-v_1^*), \exp(-v_2^*)).$$

Now (22) has the following limit

$$\begin{aligned} &\lim_{n \rightarrow \infty} n \left[1 - C_F \left(1 - \frac{v_1}{n}, 1 - \frac{v_2}{n} \right) \right] \\ &= \text{Term 1} + \text{Term 2} \\ &= -\log \left\{ \exp \left\{ -\frac{F_{\text{bulk}}(u_1, u_2)}{F_{\text{bulk}}(u_1, u_2) + [1 - F_{\text{bulk}}(u_1, u_2)]R} v_2 \right\} \times \right. \\ &\quad \left. C_G^{1 - F_{\text{bulk}}(u_1, u_2)} \left(\exp \left\{ -\frac{v_1}{1 - F_{\text{bulk}}(u_1, u_2)} \right\}, \exp \left\{ -\frac{v_2 R}{F_{\text{bulk}}(u_1, u_2) + [1 - F_{\text{bulk}}(u_1, u_2)]R} \right\} \right) \right\}. \end{aligned}$$

Define a new mapping $C_M(w_1, w_2) : [0, 1]^2 \rightarrow [0, 1]$,

$$C_M(w_1, w_2) = w_2^{c_2} C_G^{1/c_1} (w_1^{c_1}, w_2^{c_3}), \quad w_1, w_2 \in [0, 1],$$

where $c_1 = 1 / [1 - F_{\text{bulk}}(u_1, u_2)]$, $c_2 = F_{\text{bulk}}(u_1, u_2) / \{F_{\text{bulk}}(u_1, u_2) + [1 - F_{\text{bulk}}(u_1, u_2)]R\}$, $c_3 = R / \{F_{\text{bulk}}(u_1, u_2) + [1 - F_{\text{bulk}}(u_1, u_2)]R\}$, and they have the relationship $c_3 / c_1 + c_2 = 1$. We have

$$\lim_{n \rightarrow \infty} n \left[1 - C_F \left(1 - \frac{v_1}{n}, 1 - \frac{v_2}{n} \right) \right] = -\log C_M(\exp(-v_1), \exp(-v_2)).$$

One of the conditions for $C_M(w_1, w_2)$ to be a copula is $C_M(w, 1) = C_M(1, w) = w$ for all $0 \leq w \leq 1$. It can be verified that $C_M(w, 1) = w$, but

$$C_M(1, w) = w^{c_2 c_3 / c_1} = w^{(1-c_2)c_2} \neq w \quad (26)$$

for any real value c_2 . Therefore, C_M is not a valid copula; consequently, F is not in the MDA of any mGEVD G .

□

References

- Allen, S., Ginsbourger, D., and Ziegel, J. (2023). Evaluating forecasts for high-impact events using transformed kernel scores. *SIAM/ASA Journal on Uncertainty Quantification*, 11(3):906–940.
- André, L., Wadsworth, J., and O’Hagan, A. (2024). Joint modelling of the body and tail of bivariate data. *Computational Statistics & Data Analysis*, 189:107841.
- Aulbach, S., Bayer, V., and Falk, M. (2012a). A multivariate piecing-together approach with an application to operational loss data. *Bernoulli*, 18(2).
- Aulbach, S., Falk, M., and Hofmann, M. (2012b). The multivariate piecing-together approach revisited. *Journal of Multivariate Analysis*, 110:161–170.
- Barnard, J., McCulloch, R., and Meng, X.-L. (2000). Modeling covariance matrices in terms of standard deviations and correlations, with application to shrinkage. *Statistica Sinica*, 10(4):1281–1311.
- Behrens, C. N., Lopes, H. F., and Gamerman, D. (2004). Bayesian analysis of extreme events with threshold estimation. *Statistical Modelling*, 4(3):227–244.
- Beirlant, J., editor (2004). *Statistics of Extremes: Theory and Applications*. Wiley Series in Probability and Statistics. Wiley, Hoboken, NJ.
- Castellanos, M. and Cabras, S. (2007). A default Bayesian procedure for the generalized Pareto distribution. *Journal of Statistical Planning and Inference*, 137(2):473–483.

- Castro-Camilo, D., Huser, R., and Rue, H. (2019). A spliced gamma-generalized pareto model for short-term extreme wind speed probabilistic forecasting. *Journal of Agricultural, Biological and Environmental Statistics*, 24(3):517–534.
- Chan, R. K. and So, M. K. (2017). On the performance of the bayesian composite likelihood estimation of max-stable processes. *Journal of Statistical Computation and Simulation*, 87(15):2869–2881.
- Coles, S., Heffernan, J., and Tawn, J. (1999). Dependence measures for extreme value analyses. *Extremes*, 2(4):339–365.
- Coles, S. G. and Powell, E. A. (1996). Bayesian Methods in Extreme Value Modelling: A Review and New Developments. *International Statistical Review / Revue Internationale de Statistique*, 64(1):119–136.
- Davison, A. C. and Smith, R. L. (1990). Models for exceedances over high thresholds. *Journal of the Royal Statistical Society: Series B (Methodological)*, 52(3):393–425.
- de Haan, L. and Ferreira, A. (2006). *Extreme Value Theory: An Introduction*. Springer Series in Operations Research. Springer, New York ; London.
- de Valpine, P., Turek, D., Paciorek, C., Anderson-Bergman, C., Temple Lang, D., and Bodik, R. (2017). Programming with models: writing statistical algorithms for general model structures with NIMBLE. *Journal of Computational and Graphical Statistics*, 26:403–413. R package version 4.3.1.
- do Nascimento, F. F., Gamerman, D., and Lopes, H. F. (2012). A semiparametric Bayesian approach to extreme value estimation. *Statistics and computing*, 22(2):661–675.
- Frigessi, A., Haug, O., and Rue, H. (2002). A dynamic mixture model for unsupervised tail estimation without threshold selection. *Extremes*, 5(3):219–235.
- Gneiting, T. and Raftery, A. E. (2007). Strictly proper scoring rules, prediction, and estimation. *Journal of the American Statistical Association*, 102(477):359–378.
- Holzmann, H. and Klar, B. (2017). Focusing on regions of interest in forecast evaluation. *The Annals of Applied Statistics*, 11(4):2404 – 2431.

- Huang, W. K., Nychka, D. W., and Zhang, H. (2019). Estimating precipitation extremes using the log-histospline. *Environmetrics*, 30(4):e2543.
- Kiriliouk, A., Rootzén, H., Segers, J., and Wadsworth, J. L. (2019). Peaks over thresholds modeling with multivariate generalized Pareto distributions. *Technometrics*, 61(1):123–135.
- Krock, M., Bessac, J., Stein, M. L., and Monahan, A. H. (2022). Nonstationary seasonal model for daily mean temperature distribution bridging bulk and tails. *Weather and Climate Extremes*, 36:100438.
- Leonelli, M. and Gamerman, D. (2020). Semiparametric bivariate modelling with flexible extremal dependence. *Statistics and computing*, 30(2):221–236.
- Lewandowski, D., Kurowicka, D., and Joe, H. (2009). Generating random correlation matrices based on vines and extended onion method. *Journal of Multivariate Analysis*, 100(9):1989–2001.
- MacDonald, A., Scarrott, C. J., Lee, D., Darlow, B., Reale, M., and Russell, G. (2011). A flexible extreme value mixture model. *Computational statistics & data analysis*, 55(6):2137–2157.
- Naveau, P., Huser, R., Ribereau, P., and Hannart, A. (2016). Modeling jointly low, moderate, and heavy rainfall intensities without a threshold selection. *Water Resources Research*, 52(4):2753–2769.
- Opitz, T., Huser, R., Bakka, H., and Rue, H. (2018). INLA goes extreme: Bayesian tail regression for the estimation of high spatio-temporal quantiles. *Extremes*, 21(3):441–462.
- Pauli, F., Racugno, W., and Ventura, L. (2011). Bayesian composite marginal likelihoods. *Statistica Sinica*, pages 149–164.
- Pickands, J. (1975). Statistical inference using extreme order statistics. *The Annals of Statistics*, 3(1):119–131.
- Praveena, A., Srinath, S., and Ravi, S. (2019). On mixture distributions and their max domains. *Journal of the Indian Society for Probability and Statistics*, 20:173–183.

- Resnick, S. I. (1971). Tail equivalence and its applications. *Journal of Applied Probability*, 8(1):136–156.
- Ribatet, M., Cooley, D., and Davison, A. C. (2012). Bayesian inference from composite likelihoods, with an application to spatial extremes. *Statistica Sinica*, pages 813–845.
- Roberts, G. O. and Rosenthal, J. S. (2001). Optimal scaling for various Metropolis-Hastings algorithms. *Statistical Science*, 16(4).
- Rootzén, H., Segers, J., and L. Wadsworth, J. (2018). Multivariate peaks over thresholds models. *Extremes*, 21(1):115–145.
- Rootzén, H. and Tajvidi, N. (2006). Multivariate generalized Pareto distributions. *Bernoulli*, 12(5):917–930.
- Segers, J. (2012). Max-stable models for multivariate extremes. *Revstat Statistical Journal*, 10.
- Sibuya, M. (1960). Bivariate extreme statistics, I. *Annals of the Institute of Statistical Mathematics*, 11(3):195–210.
- Smith, E. L. and Stephenson, A. G. (2009). An extended gaussian max-stable process model for spatial extremes. *Journal of Statistical Planning and Inference*, 139(4):1266–1275.
- Stein, M. L. (2021). A parametric model for distributions with flexible behavior in both tails. *Environmetrics*, 32(2):e2658.
- Sun, D. and Berger, J. O. (2007). Objective bayesian analysis for the multivariate normal model. *Bayesian Statistics*, 8:525–562.
- Tancredi, A., Anderson, C., and O’Hagan, A. (2006). Accounting for threshold uncertainty in extreme value estimation. *Extremes*, 9:87–106.
- Tibbits, M. M., Groendyke, C., Haran, M., and Liechty, J. C. (2014). Automated factor slice sampling. *Journal of Computational and Graphical Statistics*, 23(2):543–563.
- Yun, S. (1997). On domains of attraction of multivariate extreme value distributions under absolute continuity. *Journal of Multivariate Analysis*, 63(2):277–295.